RSC Advances

ROYAL SOCIETY OF CHEMISTRY

www.rsc.org/advances

Table of Contents

Highlights:

Vanadium phosphates, prepared by electrochemical de-lithiation of $Li_3V_2(PO_4)_3$, are investigated as high-voltage (~ 3.0 V vs. Mg/Mg^{2+}) cathode hosts for Mg^{2+} (de)-intercalation. The exceptional high voltage surpasses hitherto reported values of cathode materials for magnesium batteries.

Graphical abstract:

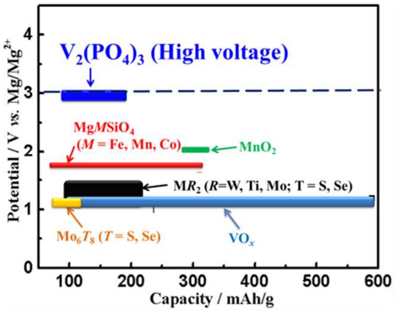

Cite this: DOI: 10.1039/c0xx00000x

www.rsc.org/xxxxxx

ARTICLE TYPE

Vanadium phosphate as a promising high-voltage magnesium ion (de)-intercalation cathode host

Zhen-Dong Huang[a,b],* Titus Masese[b], Yuki Orikasa[b], Takuya Mori[b], kentarou Yamamoto[b]

[a] Key Laboratory for Organic Electronics and Information Displays & Institute of Advanced Materials(IAM), National Synergistic Innovation Center for Advanced Materials (SICAM), Nanjing University of Posts & Telecommunications, 9 Wenyuan Road, Nanjing 210023, China

[b] Graduate School of Human and Environmental Studies, Kyoto University, Yoshida-nihonmatsu-Cho, Sakyo-ku, Kyoto 606-8501 Japan

Magnesium batteries (MBs) have been considered as one of the most promising safe and low cost energy storage systems. Herein, vanadium phosphates, prepared by electrochemical de-lithiation of $Li_3V_2(PO_4)_3$, are investigated as a high-voltage cathode host for Mg^{2+} (de)-intercalation. The reversible (de)-intercalation of Mg^{2+} into (from) the host structure of $V_2(PO_4)_3$ are verified by the comprehensive analysis of the results from the electrochemical tests, synchrotron X-ray diffraction and absorption, and inductively coupled plasma measurements. Its exceptional high average working voltage (~ 3.0 V *vs.* Mg/Mg^{2+}) surpasses other reported values of cathode hosts for MBs.

Prime attention has been inclined towards developing alternative energy storage devices which have comparable electrochemical performance, but safer and of much lower cost than lithium ion batteries, in order to meet the escalating new energy demand in futures low carbon society. Mg batteries have gained considerable concerns since the development of a prototype rechargeable Mg battery, where Mg^{2+} ions replace Li^+ as the charge carrier, in 2000. [1] Compared to Li anode, Mg anode shows much lower cost (3020 \$ ton^{-1}, *vs.* ~ 69000 \$ ton^{-1} for Li), much higher abundance (13.9 %, *vs.* 7 × 10^{-4} % for Li) and higher theoretical volumetric energy density (3832 mAh cm^{-3}, *vs.* 2062 mAh cm^{-3} for Li). [1, 2] Moreover, Mg is stable upon air exposure and is free of dendritic deposition during repeated cycling, thus, inherently safer than Li. [1, 2] Although Mg batteries are deemed as promising alternatives for a gamut of large-scale storage devices that could couple with renewable energy sources to load the electric grid, the low working voltage as well as low capacity of the cathode material limits the attainable energy; thereby, hampering the commercial realization of Mg batteries. [3] One of the most effective and direct solutions is to find a proper cathode host with a high average working voltages as well as high capacities.

Up to date, as shown in Table S1, only several cathode materials, including Chevrel phases $A_xMo_6T_8$ (A = metal, T = S, Se) [4, 5] Mg_xMSiO_4 (M = Fe, Mn, Co), [6-9] transition metal oxides (V_2O_5, [10-14] MnO_2 [15-17]) and transition metal chalcogenides (MoS_2, TiS_2 and WSe_2), [18-21] have been reported as feasible cathode materials for Mg batteries which exhibit reasonable reversible capacities. Much effort has been devoted to bypassing the intrinsically sluggish solid-state diffusion of Mg^{2+} within the host cathodes via morphological design strategies, such as nano-sizing and carbon-coating [18-21] However, most of the reported cathode materials show relatively low working voltages (see Table S1). Therefore, the pursuit for novel high voltage cathode materials that exhibit high capacity is crucial for the development of high energy density Mg battery systems.

Vanadium phosphates (*viz.*, $Li_3V_2(PO_4)_3$ (hereafter denoted as LVP)) has proved to be promising high performance cathode materials for lithium ion batteries, due to their high working voltage (~ 4 V), high theoretical capacity (197 mAh g^{-1}), three-dimensional (3D) crystal structural framework, good thermal stability and remarkable rate capability. [22-24] It was reported that the average working potential of Mg^{2+}-based compounds *vs.* Mg/Mg^{2+} was about 1 V lower than that of their Li^+-based analogues in lithium ion battery systems. [2] Thus, the expected average working voltage of $Mg_xV_2(PO_4)_3$ (the Mg^{2+} intercalated counterparts of LVP) could be up to ~ 3 V, which is much higher than the reported cathode materials shown in Table S1. Therefore, we anticipate to employ LVP and/or $Mg_xV_2(PO_4)_3$ as high voltage cathode materials to couple with Mg anode. Worthy to mention is that, to date, no attention has been paid to exploring the $A_xV_2(PO_4)_3$ system (where A = Li, Na ($0 \leqslant x \leqslant 3$) or Mg ($0 \leqslant x \leqslant 1.5$)) as potential cathode materials for Mg batteries.

In this communication, we report on the feasibility of using electrochemically delithiated $V_2(PO_4)_3$ (hereafter denoted as ED-VP) as a promising magnesium ion (de)-intercalation host and provide promising high voltage cathode host material contenders for Mg batteries. Here, ED-VP was prepared by electrochemical delithiation of all three lithiums from the host structure of carbon-coated $Li_3V_2(PO_4)_3$ (hereafter denoted as C-LVP). Electrochemical measurements, crystal and electronic structural as well as composition analyses indicate that ED-VP demonstrate exceptionally high average working voltage with reasonable capacity in Mg^{2+} electrolyte. Reversible Mg^{2+} (de)-intercalation into (from) the host frameworks of ED-VP have been verified by our findings.

Figure 1 shows the Scanning Electron Microscopy (SEM) images and synchrotron X-ray diffraction (SXRD) patterns of pristine C-LVP. Citric acid and high surface area carbon (Ketjen black) were used as carbon source for the carbothermal reduction process.[25] The total carbon content obtained from trace elements analysis was ~ 4.1 *wt*.%. The SEM images shown in Figures 1a and 1b indicate a uniform C-LVP composite. The particle size of LVP is in the ranges of 150 − 400 nm. Figure 1c presents the Rietveld refinement of the SXRD pattern and inset shows a 3D graphical representation of the crystal structure of as-prepared LVP. The observed pattern coincides with the calculated pattern with low reliability factors, validating the quality of the fit. The lattice parameters of the as-prepared C-LVP (a = 8.6080(2) Å; b = 8.5939(2) Å; c = 14.7263(4) Å; β = 125.180(1) °) are much closer to that reported for LVP. [26] The atomic parameters are listed in Table S2 in the supplementary information (SI). Isostructural to the monoclinic structure of $Li_3Fe_2(PO_4)_3$ ($P2_1/c$ space group), LVP entails VO_6 octahedrons and PO_4 tetrahedrons which share their apical O atoms to form a 3D framework. The positions of the Li^+ ions in the empty channels (voids) vary depending on the synthesis conditions. [26]

The as-prepared C-LVP composite electrodes were electrochemically delithiated using both two-electrode Li cells and three-electrode Mg cells. The electrochemical measurements were performed at 55°C, in order to fully delithiate the three Li^+ from LVP. Figure 2a shows the initial charge profile of C-LVP in Li cell, which corresponds to the delithiation of LVP. Four typical two-phase plateaus observed at ~ 3.592 V, ~ 3.679 V, ~ 4.075 V and ~ 4.489 V, respectively, correspond to the extraction of Li^+ from three different crystallographic sites of LVP. [22, 24] The initial charge capacity of LVP is 197 mAh g^{-1}, which indicates that all three Li^+ ions have been fully extracted from LVP host structure. A similar initial charge profile with four two-phase plateaus exhibiting a charge capacity of 197 mAh g^{-1} is also observed during the initial charge process of LVP in a three-electrode Mg cell (see Figure 2b).

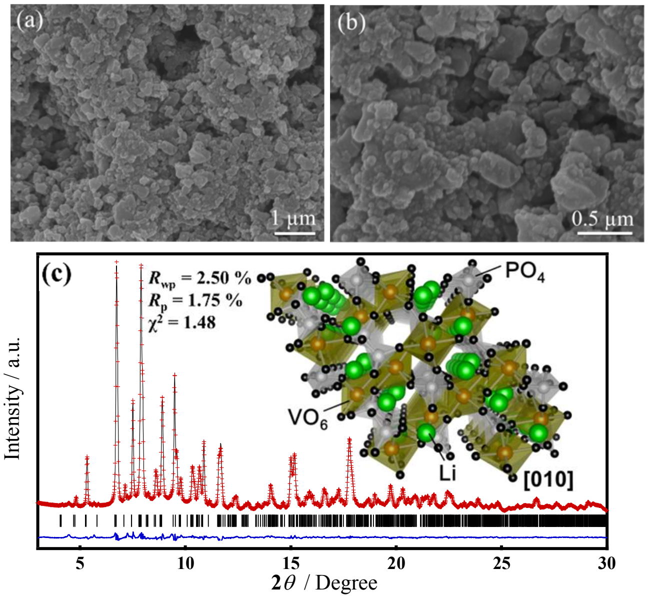

Figure 1. SEM images of as-prepared C-LVP composite: (a) × 15000, (b) ×40000; (c) Rietveld refinement of SXRD pattern of C-LVP and a 3D graphical representation of the crystal structure (inset). The wavelength was set at 0.49971 (1) Å. The observed and calculated peaks are indicated in red and black, respectively. The difference between the observed and calculated intensity is indicated in blue, while black ticks indicate the position of the Bragg peaks of the phase. The agreement indices used are $Rwp = [\Sigma wi(y_{io} - y_{ic})^2 / \Sigma wi(y_{io})^2]^{1/2}$, $Rp = \Sigma|y_{io} - y_{ic}| / \Sigma y_{io}$ and the goodness of fit, $\chi^2 = [R_{wp}/R_{exp}]^2$ where $R_{exp} = [(N - P) / \Sigma w_i y_{io}^2]^{1/2}$, y_{io} and y_{ic} are the observed and calculated intensities, wi is the weighting factor, N is the total number of y_{io} data when the background is refined, and P is the number of adjusted parameters.

The results shown in Figures 2a and 2b indicate that the as-prepared C-LVP composite can be fully delithiated in both Li and Mg cells at a current density corresponding to C/20 rate at 55°C. It is worth noting that a similar charge behaviour of LVP, but lower capacity, can be observed when the tests were conduct at room temperature. Upon delithiation of all three Li^+, the crystallinity of ED-VP apparently decreases (see the SXRD pattern of fully charged LVP in Figure S1). This observation is in line with the previous report. [23] For the sake of clarity, the four delithiation plateau voltages *vs.* Li/Li^+ were also used to calibrate the potential of LVP and ED-VP working electrodes *vs.* Ag/Ag^+ and Mg/Mg^{2+}.

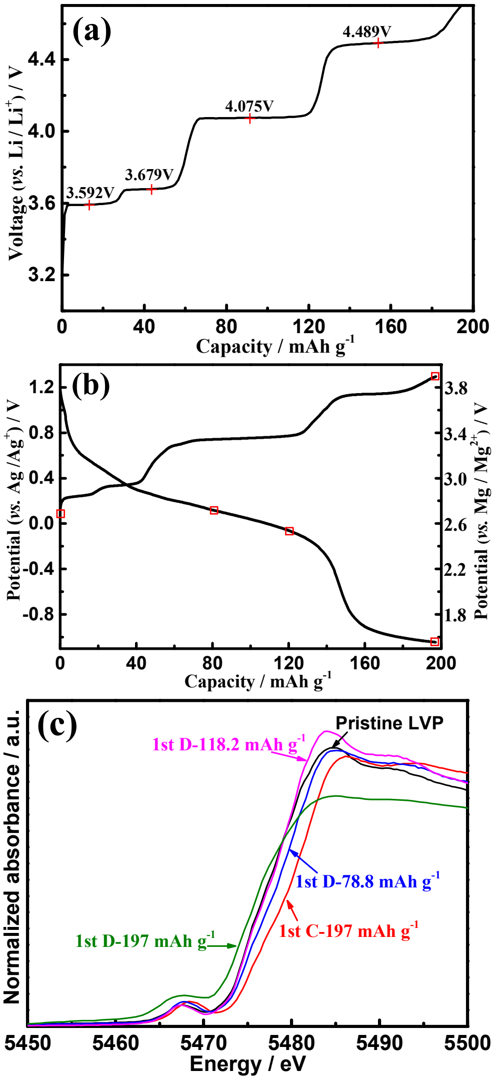

Figure 2. Electrochemical performance of the composite electrodes consisting of LVP (75 *wt.*%), carbon (15 *wt.*%) and polytetrafluoroethylene (10*wt.*%): (a) the 1st charge profile corresponding to the de-lithiation process of LVP in two-electrode Li cells, (b) the 1st charge / discharge profiles in three-electrode Mg cells using Ag/Ag^+ electrode as reference electrode, and (c) shift of X-ray absorption V-*K* absorption edges during the 1st discharge

process from the fully charged state (1st C-197 mAh g^{-1}) to the fully discharged state (1st D-197 mAh g^{-1}).

In this work, galvanostatic measurements were conducted for both C-LVP and ED-VP working electrodes in a three-electrode Mg ion cell using Ag/Ag^+ standard electrode and Mg rod as reference and counter electrode, respectively. 0.5 M $Mg(TFSI)_2$ in acetonitrile solution was used as the electrolyte. Figure S2 shows the electrochemical performance of LVP with repeated cycling. Surprisingly, the attained discharge capacity of LVP electrode is 197mAh g^{-1} within the same three-electrode Mg cells. Moreover, the average (dis)charge potential is around 3.0 V *vs.* Mg/Mg^{2+} determined according to both the delithiation potential *vs.* Li/Li^+ anode and the reference potential *vs.* Ag/Ag^+, which further confirms that the voltage expected with a Mg battery is about 1V lower than that of a lithium ion battery using the same cathode materials.[2] It is notable that the average working voltage *vs.* Mg/Mg^{2+} (~ 3.0 V) and the reasonable capacity (197 mAh g^{-1}) of LVP outclasses hitherto reported cathode host materials for rechargeable MBs (refer to Table S1). Furthermore, two plateaus were observed when the cell was discharged to 197 mAh g^{-1} (see Figure 2b). Interestingly, during the subsequent cycles, the quasi plateau charge profiles (typical of a two-phase electrochemical behaviour) gradually transform to sloping single-phase profiles (Figure S2), due to the gradually decreasing contribution from Li^+ intercalation and slight structure variation caused by the intercalation of Mg^{2+}.

Figure 2c shows the shifts of the absorption edges of the V-*K* edge XAS spectra, which correspond to the oxidation or reduction of vanadium ions; this is a univocal evidence for the intercalation of Mg^{2+} and Li^+ during the discharge process. Further intercalation of more Mg^{2+} and Li^+ into the outer layer of LVP active particles should be accounted for the further shift of V-*K* edge absorption spectra to lower absorption energy beyond that of pristine LVP upon discharging to 197 mAh g^{-1}. This phenomenon does not come entirely as a surprise, taking into account the sluggish diffusion kinetics of Mg^{2+} and the multivalent nature of vanadium ions.

As shown in Figure S1, the crystallinity of delithiated LVP recovered in a certain degree with the varying amount of inserted Mg^{2+} and/or Li^+. For example, the electrode discharged to a capacity of 118.2 mAh g^{-1} exhibits the highest crystallinity in the same monoclinic $P2_1/c$ space group as LVP. Its refined SXRD pattern and 3D graphical representation of the crystal structure are presented in Figure 3. The refined atomic coordinates are furnished in Table S3. The composition formula estimated from the Rietveld refinement is $Li_{0.7}Mg_{0.55}V_2(PO_4)_3$, which is slightly different from the composition formula calculated based on the results of the ICP measurements shown in Table S4. The calculated composition formulas for the electrodes discharged to a capacity of 78.8 mAh g^{-1} and 118.2 mAh g^{-1} are $Li_{1.32}Mg_{0.37}V_2(PO_4)_3$ and $Li_{1.35}Mg_{0.44}V_2(PO_4)_3$, respectively. These observations are unambiguous proofs that Mg^{2+} have been successfully intercalated into the structural framework of electrochemically de-lithiated $V_2(PO_4)_3$. The discrepancy in the composition predicted by structural refinement and ICP measurement should be caused by the non-uniform composition from surface to core of active particles. More Mg^{2+} should be found from the outer layer of the particles due to the much slower diffusion kinetics of Mg^{2+} than Li^+. Both the ICP analysis results and the over shift of V *K*-edge absorption spectra reveal that the discharge plateau observed at low potential arises from further intercalation of Mg^{2+} and Li^+ into the outside layer, rather than the decomposition of electrolyte.

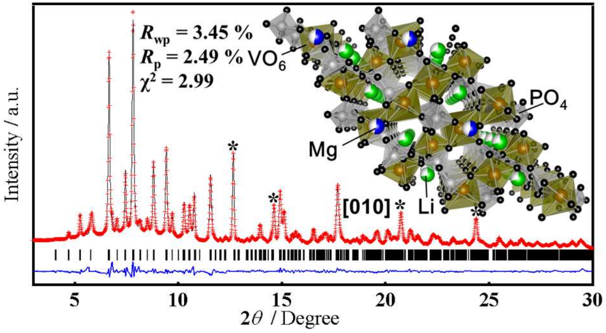

Figure 3. Rietveld refinement SXRD pattern for the electrode discharged to 118.2 mAh g^{-1} (1st D-118.2). Inset depicts a 3D graphical representation of the crystal structure. The wavelength was set at 0.49971(1) Å. The observed and calculated peaks are indicated in red and black, respectively. The difference between the observed and calculated intensity is indicated in blue, while black ticks indicate the position of the Bragg peaks of the phase. Peaks arising from Pt metal (current collector) which overlapped with the observed peaks are indicated in asterisks and were excluded from the refinement.

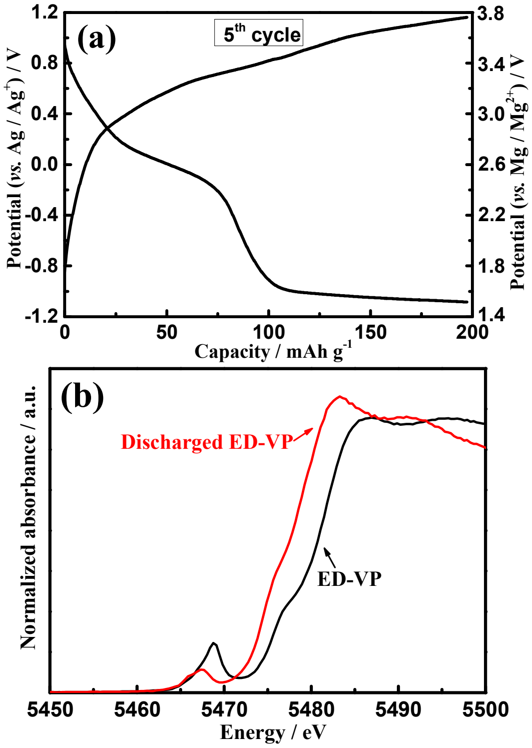

Figure 4. (a) The 5th discharge/charge profile at ~10 mA g^{-1}, (b) the 7th cyclic voltammetry curve of $V_2(PO_4)_3$ electrodes obtained by the electrochemical delithiation of $Li_3V_2(PO_4)_3$ electrodes (ED-VP) within newly assembled three-electrode cells at a scanning rate of 0.1 mV s^{-1} and (c) shift of X-ray absorption V-*K* edge spectrum to low energy during the 1st discharge process of ED-VP. The electrochemical measurements were conducted at 55°C in the three

electrode Mg cells. Starting from 5th cycle, the charge/discharge profile of ED-VP is similar with that of LVP (see Figures S2 and S3). Additionally, the initial two oxidation peaks merge into one broad peak starting from the 7th cyclic voltammogram of ED-VP.

The decreasing discharge capacity of the high potential discharge plateau with cycling should be ascribed to the decreasing intercalation of Li$^+$. As presented in Table S5, the lattice parameters and lattice volume obviously increase with the rise of discharge capacity, in other words, with the intercalation of more Li$^+$ and Mg^{2+}.

To investigate the (de)intercalation behaviour of Mg^{2+} within the host structure of ED-VP and avoid the influence of Li$^+$, the fully delithiated ED-VP electrodes were characterized using newly assembled three-electrode Mg cells after being washed several times with acetonitrile. Figure 4 shows the galvanostatic discharge/charge profiles (5th cycle) of ED-VP electrodes. With respect to the discharge process of ED-VP electrodes in Mg^{2+} electrolyte, an obvious transfer of discharge profiles from an initially linear profile to a sloping stage profile could be observed from Figure S3, which indicates that the discharge behaviour changed from surface absorption and outer layer insertion of Mg^{2+} to 'inner core' diffusion of Mg^{2+}. Two discharge plateaus are observed from the 5th discharge profile (see Figure 4a). The initial charge profile exhibits a typically short flat plateau; however, the subsequent charge profiles gradually change to long sloping profiles. The charge capacity also increased to 197 mAh g^{-1} at the 5th cycle. From the 5th cycle, the electrochemical performance of ED-VP electrodes were the same as for the LVP electrodes cycled in Mg^{2+} electrolyte, as shown in Figure S2 and Figure 4a. Generally speaking, the consistent evolutions of charge/discharge profiles indicate that reversible intercalation/de-intercalation of Mg^{2+} into/from the ED-VP electrode is gradually activated during the initial 5 cycles. The apparent shift to lower energies of the absorption edge features for V-*K* edge XAS spectra, corresponds to the reduction of vanadium ions during the initial discharge process of ED-VP (Figure 4b). This validates the intercalation of Mg^{2+} during the discharge process.

Additionally, the CV measurement have been done to further discuss the (de)intercalation mechanisms. Figure 5a depict the cyclic voltammetry (CV) curves of LVP cathode material in a three-electrode Mg cell. Four sharp oxidation peaks are observed in the initial cycle, which are indicative of the four two-phase plateaus observed during the initial delithiation process. The gradual transformation of electrochemical behaviour from a two- to single-phase is also evident, as manifested by the weakening and broadening of the oxidation peaks. The broad reduction peaks and the sloping discharge profiles are reminiscent of a single-phase electrochemical behaviour. With subsequent cycling, the transitions between 1st and 2nd reduction peaks become smoother, while the 2nd reduction peaks become narrow and the 3rd reduction peak is more distinct. These observations clearly reflect the smoother transition from initial discharge profile to the gradually shorter discharge plateau at high potentials, and the extension of the discharge plateau at low potentials. Based on the stabilized CV curves shown in Figure 5a, we expect the charge carriers (Mg^{2+} and/or Li$^+$) to be reversibly inserted into and extracted from the host structure of delithiated LVP.

The evolution of the CV curves of ED-VP with successive cycling (see Figure 5b) is consistent with the evolution of the galvanostatic charge/discharge profiles of ED-VP. Two sharp oxidation peaks observed from the 1st cycle of the CV curve diminish in the subsequent cycles, and the subsequent oxidation peaks slightly shifted to lower potential and become broader. Starting from 7th cycle, the oxidation peaks centered at different potentials merged into a broad peak. Indifferent to ED-VP, three distinct oxidation peaks were observed from the CV curves of the LVP electrodes in Mg^{2+} electrolyte (see Figure 5a). This difference indicates that the oxidation peaks centered at ~ 0.24 V and 0.34 V correspond to the extraction of Li$^+$ from the structure of discharged LVP in Mg^{2+} electrolyte. Moreover, the shaper oxidation peak centered at ~ 0.8 V and the slightly higher average working potential (~ 3.0 V *vs.* Mg/Mg^{2+}) of LVP than that of ED-VP (~ 2.9 V *vs.* Mg/Mg^{2+}) are due to faster transfer kinetics and the more positive chemical potential of Li$^+$ than that of Mg^{2+} in the same hosts. [2] Initially, a reduction peak centered at ~ 0.8 V is observed. Subsequently, the reductive peak gradually broadens and shifts to ~ 0.62 V. Starting from the 4th cycle, two additional broad oxidation peaks centered at

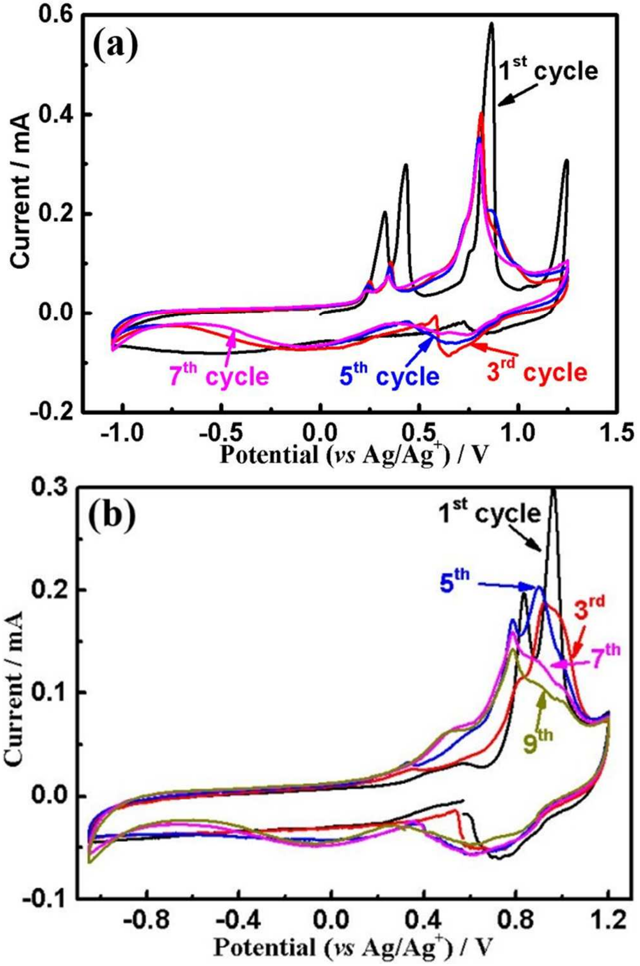

Figure 5. (a) the evolution of cyclic voltammograms during the initial 7 cycles of LVP in three-electrode Mg cells and (b) the cyclic voltammograms of $V_2(PO_4)_3$ electrodes obtained via the electrochemical delithiation of $Li_3V_2(PO_4)_3$ electrodes (ED-VP) using newly assembled three-electrode cells at a scanning rate of 0.1 mV s^{-1} at 55 °C, respectively.

~ −0.06 V and ~ −1.05 V emerge from the 4th and 7th cycles, respectively. The cyclic voltammograms of ED-VP electrode are the same as that of LVP electrode tested in Mg^{2+} electrolyte (Figures 5a and 5b). Generally speaking, the consistent evolutions of both charge/discharge profiles and CV curves indicate that reversible intercalation/de-intercalation of Mg^{2+} into/from the ED-VP electrode is gradually activated during the initial 5 cycles.

In summary, $Li_3V_2(PO_4)_3$ (LVP) was prepared by using a ball-milling-assisted solid state carbothermal method. All three lithium ions were electrochemically delithiated from LVP to successfully prepare $V_2(PO_4)_3$ (ED-VP). Electrochemical measurements, coupled with crystal structure, electronic structure and composition analyses validate that Mg^{2+} can be reversibly intercalated into and extracted from the host structure of ED-VP. As cathode host materials for Mg batteries, both LVP (~ 3.0 V) and ED-VP (~ 2.9 V) exhibit high average working voltages *vs.* Mg/Mg^{2+} with a reasonable high capacity (*i.e.,* 197 mAh g^{-1}). To the best of our knowledge, the exhibited voltage by far surpasses other reported cathode materials for Mg batteries. This work not only provides a high-voltage cathode material contender for the Mg battery systems, but also highlights the versatility of electrochemical cation exchange for accessing new functional materials for futures rechargeable battery systems. Further work is ongoing to understand the evolution of the crystal structure and electrochemical behaviour of LVP and VP as high-rate cathode materials for Mg batteries. Additionally, a stable electrolyte, which is compatible to Mg anode and possessing a wide voltage window of 0~4 V, or even 0~5 V, should be developed in order to develop high performance prototype two-electrode Mg batteries by using $V_2(PO_4)_3$-based compounds, such as LVP and ED-VP, as cathode materials.

This work was supported by the Core Research for Evolutional Science and Technology (CREST) project of the Strategic Basic Research Programs of Japan Science and Technology Agency (JST).

Notes and references

[a] *Key Laboratory for Organic Electronics and Information Displays & Institute of Advanced Materials(IAM), National Synergistic Innovation Center for Advanced Materials (SICAM), Nanjing University of Posts & Telecommunications, 9 Wenyuan Road, Nanjing 210023, China*
Email: hzd0506127@gmail.com
[b] *Graduate School of Human and Environmental Studies, Kyoto University, Yoshida-nihonmatsu-Cho, Sakyo-ku, Kyoto 606-8501 Japan*

Electronic Supplementary Information (ESI) available: [details of experimental process and additional results are included here]. See DOI:10.1039/b000000x/

1 D. Aurbach, Z. Lu, A. Schechter, Y. Gofer, H. Gizbar, R. Turgeman, Y. Cohen, M. Moshkovich, E. Levi, Nature, 2000, 407, 724.
2 E. Levi, Y. Gofer and D. Aurbach, Chem. Mater., 2010, 22, 860.
3 H. S. Kim, T. S. Arthur, G. D. Allred, J. Zajicek, J. G. Newman, A. E. Rodnyansky, A. G. Oliver, W. C. Boggess, J. Muldoon, Nat. Commun., 2011, 2, 427.
4 A. Mitelman, M. D. Levi, E. Lancry, E. Levi, D. Aurbach, Chem. Commun., 2007, 4212.
5 E. Lancry, E. Levi, Y. Gofer, M. D. Levi, D. Aurbach, J. Solid. State. Electrochem., 2005, 9, 259.
6 Y. Li, Y.N. Nuli, J. YANG, T. Yilinuer, J. L. Wang, Chinese Sci. Bull., 2011, 56, 4.
7 Y.N. NuLi, J. Yang, Y.S. Li and J.L. Wang, Chem. Commun., 2010, 46, 3794.
8 Z. Feng, J. Yang, Y.N. NuLi, J.L. Wang, J. Power Sources, 2008, 184, 604.
9 Y.P. Zheng, Y.N. NuLi, Q. Chen, Y. Wang, J. Yang, J.L. Wang, Electrochim. Acta, 2012, 66, 75.
10 L.F. Jiao, H.T. Yuan, Y.C. Si, Y.J. Wang, J.S. Cao, X.L. Gao, M. Zhao, X.D. Zhou, Y.M. Wang, J. Power Sources, 2006, 156, 673.
11 L. F. Jiao, H.T. Yuan, Y.C. Si, Y.J. Wang, Y.M. Wang, Electrochem. Commun., 2006, 8, 1041.
12 L. Yu, X. Zhang, J. Colloid Interface Sci., 2004, 278, 160.
13 D. Imamura, M. Miyayama, Solid State Ionics, 2003, 161, 173.
14 D. Imamura, M. Miyayama, M. Hibino, T. Kudo, J. Electrochem. Soc., 2003, 150, A753.
15 R.G. Zhang, X.Q. Yu, K.W. Nam, C. Ling, T.S. Arthur, W. Song, A.M. Knapp, S.N. Ehrlich, X.Q. Yang, M. Matsui, Electrochem. Commun., 2012, 23, 110.
16 S. Rasul, S. Suzuki, S. Yamaguchi, M. Miyayama, Solid State Ionics, 2012, 225, 542.
17 S. Rasul, S. Suzuki, S. Yamaguchi, M. Miyayama, Electrochim. Acta, 2012, 82, 243.
18 Y.L. Liang, R.J. Feng, S.Q. Yang , H. Ma, J. Liang, J. Chen, Adv. Mater., 2011, 23, 640.
19 Y.C. Liu, L.F. Jiao, Q. Wu, Y.P. Zhao, K. Z. Cao, H.Q. Liu, Y. J. Wang, H.T. Yuan, Nanoscale, 2013, 5, 9562.
20 Z.L. Tao, L.N. Xu, Xi.L. Gou, J. Chen, H.T. Yuan, Chem. Commun., 2004, 2004, 2080.
21 B. Liu, T. Luo, G.Y. Mu, X.F. Wang, D. Chen, G.Z. Shen, ACS Nano, 2013, 7, 8051.
22 J. Kim, J.K. Yoo, Y.S. Jung, K. Kang, Adv. Energy Mater., 2013, 3, 1004.
23 S.C. Yin, H. Grondey, P. Strobel, M. Anne, L.F. Nazar, J. Am. Chem. Soc., 2003, 125, 10402.
24 H.D. Liu, P. Gao, J.H. Fang, G. Yang, Chem. Commun., 2011, 47, 9110.
25 Z.D. Huang, Y. Orikasa, T. Masese, K. Yamamoto, T. Mori, T. Minato, Y. Uchimoto, RSC Adv., 2013, 3, 22935.
26 Y. Kee, H. Yun, Acta Cryst., 2013, E69, i11.